Distribution and Quantity of Contractile Tissue in Postnatal Development of Rat Alveolar Interstitium

RENÉE DICKIE,[1]* YVES T. WANG,[1] JAMES P. BUTLER,[1] HOLGER SCHULZ,[2] AND AKIRA TSUDA[1]

[1]Molecular and Integrative Physiological Sciences, Dept. of Environmental Health, Harvard School of Public Health, Boston, Massachusetts

[2]GSF- National Research Center for Environment and Health, Institute for Inhalation Biology, Neuherberg/München, Germany

ABSTRACT

Alpha–smooth muscle actin (α-SMA) -expressing cells are important participants in lung remodeling, during both normal postnatal ontogeny and after injury. Developmental dysregulation of these contractile cells contributes to bronchopulmonary dysplasia in newborns, and aberrant recapitulation in adults of the normal ontogeny of these cells has been speculated to underlie disease and repair in mature lungs. The significance of airway smooth muscle has been widely investigated, but contractile elements within the pulmonary parenchyma, although also of structural and functional consequence in developing and mature lungs, are relatively unstudied and little quantitative information exists. Here, we quantify the areal density of α-SMA expression in lung parenchyma and assess changes in its spatiotemporal distribution through postnatal ontogeny. Using an antibody against α-SMA, we immunofluorescently labeled contractile elements in lung sections from a postnatal growth series of rats. Images were segmented using thresholded pixel intensity. Alpha-SMA areal density in the alveolar interstitium was calculated by dividing the area of α-SMA–positive staining by the tissue area. The areal density of α-SMA in 2-day neonates was 3.7%, almost doubled, to 7.2% by 21 days, and decreased to 3% in adults. Neonates had large, elongate concentrations of α-SMA, and α-SMA localized both at septal tips and within the interstitium. In adults, individual areas of α-SMA expression were smaller and more round, and located predominately in alveolar ducts, at alveolar ends and bends. The results are consistent with increasing α-SMA expression during the period of peak myofibroblast activity, corresponding to the phase of rapid alveolarization in the developing lung. Anat Rec, 291:83–93, 2007.

Key words: alveolar septa; myofibroblast; smooth muscle actin; postnatal lung

Grant sponsor: NIH; Grant numbers: HL070542, HL074022 and HL054885.

*Correspondence to: Renée Dickie, Molecular and Integrative Physiological Sciences, Department of Environmental Health, Harvard School of Public Health, 665 Huntington Ave., Boston, MA 02115. Fax: 617-432-3468.

E-mail: rdickie@hsph.harvard.edu

Received 1 March 2007; Accepted 18 October 2007

DOI 10.1002/ar.20622

Published online in Wiley InterScience (www.interscience.wiley.com).

The majority of studies of contractile tissue within the lung have focused on the role of smooth muscle in airways and large blood vessels, but contractile elements are also found within the alveolar parenchyma. Their role as contractile tissue is unclear, insofar as the stress-bearing structures within the lung, including both connective tissue and surfactant-associated surface tension at the air–liquid interface, do not require contractility per se to support the appropriate pressure/volume characteristics of the lung. Nevertheless, it is clear that one important consequence of the presence of contractile tissue in the pulmonary parenchyma is in the alveolarization stage of postnatal development, and by hypothesis, a potential common pathway between development and remodeling and repair in the adult lung. Alpha–smooth muscle actin (α-SMA) -expressing myofibroblasts are associated with regions and periods of developmental remodeling (Mitchell et al., 1990). For example, they are essential for the secondary septation that forms alveoli (Kim and Vu, 2006). Mice deficient in platelet-derived growth factor A (PDGF-A−/−) lack α-SMA and alveolar myofibroblasts. They develop an emphysema-like morphology as alveolar septa fail to form (Bostrom et al., 1996; Lindahl et al., 1997).

The link between normal, morphogenetic lung development and abnormal disease-associated lung remodeling is an area of active inquiry (Demayo et al., 2002). Warburton et al. (2001) speculate that lung remodeling and repair may use the same pathways as those of normal development. Developmental dysregulation of myofibroblasts contributes to bronchopulmonary dysplasia (BPD), a chronic lung disease characterized by airway obstruction and defective gas exchange (Bourbon et al., 2005). Torday and Rehan (2007) have suggested that the fibroblast-to-myofibroblast differentiation associated with BPD pathogenesis in newborns, and with chronic lung disease in adults, represents an ontogenetic recapitulation of myofibroblast development. Similarly, Rishikof et al. (2006), using an elastase model of emphysema in mice, speculate that the damaged areas of the lung represent a reactivation of the myofibroblast proliferation and increased α-SMA content normally associated with postnatal alveolar septation. More detailed characterization of α-SMA expression during normal lung development thus would appear to be a well-motivated first step in evaluating these proposed ontogenetic recapitulations.

Despite its structural, functional, and developmental importance, relatively little is known about smooth muscle ontogeny of the lung during normal mammalian development (McHugh, 1995). We are particularly interested in its role in postnatal development of the rat lung, given the similarities between major events of lung development in this species and many other mammals, including humans. Although the stages of lung development are similar across species, mammals vary in the degree of lung maturity that is present at birth. Compared to humans, which begin alveolarization during gestation, in rats the formation of alveoli occurs relatively late, making them a convenient model with which to study events associated with secondary septation. The majority of alveolarization takes place between postnatal day 4 and 13 (Burri, 2006), while maturation and thinning of the septa occur mainly during the third week (Schittny et al., 1998). We hypothesize that the peak ratio of α-SMA–positive tissue to total tissue would occur in the third week, when the myofibroblast content is still high from the preceding period of bulk alveolarization, but parenchymal tissue density has diminished.

Alpha-SMA antibody, in addition to labeling smooth muscle cells and microvascular pericytes, is the most reliable marker of myofibroblasts (Skalli et al., 1986, Tomasek et al., 2002). The distribution of α-SMA has recently been described qualitatively in a rat growth series (Yamada et al., 2005), but little is known concerning quantifiable changes in α-SMA content within the alveolar septa in the postnatal developing lung. Such quantitative structural data are required to accurately model age-related changes in lung function at the level of the acinus (Kojic et al., 2006) and to help evaluate proposed recapitulative similarities in the pathogenesis of lung disease and the normal ontogenetic course.

To better understand the changes in parenchymal SMA content that accompany lung maturation, our study sought to relate the abundance and spatial and temporal distribution of α-SMA in the alveolar septa to the different developmental stages of the postnatal rat lung. The areal density of α-SMA immunofluorescence was calculated from parenchymal images of the left lung acquired by confocal microscopy. The present study extends previous qualitative descriptions of the immunolocalization of α-SMA in alveolar parenchyma, and provides a quantitative measure of the changes in α-SMA content that accompany maturation.

MATERIALS AND METHODS

Experimental Animals

The details of lung growth in some rodents are known to vary by strain (Le Cras et al., 1999; Soutiere and Mitzner, 2006); we used the outbred Wistar rat (Crl:WI) strain obtained from Charles River Laboratories (Wilmington, MA) in all of our experiments. Rats, rather than mice, were used because their larger lungs allowed for better fixation in the inflated state in the neonates.

The animals were maintained on a 12-hr light/dark cycle in microinsulator cages within the animal care facility of the Harvard School of Public Health. The rats were allowed commercial stock food pellets and water ad libitum. The animals were treated in accordance with all local, state, federal and institutional guidelines and consistent with animal protocols approved by the Animal Care and Use Committee overseeing the School of Public Health.

The experimental time points for the killing of the animals were selected to preferentially sample periods of rapid developmental restructuring of the lung. For the growth series, the lungs from a minimum of five animals/time point were collected at postnatal day 2, 7, 14, 21, and 35. Rats reach sexual maturity at 40 to 60 days (Kohn and Clifford, 2002). Five mature adults (∼15 weeks) were also examined. The postnatal series of rats less than 21 days old was obtained using seven litters. This many litters were used to minimize litter-size effects on growth. Litter size ranged between 10 and 12 pups. Offspring were weaned from their mothers at 21 days. Up to 21 days of age, no distinction was made regarding the sex of the animals, because growth rate and lung development is not thought to differ significantly between the sexes up to that point (Burri et al.,

1974). Adult rats were all female; male rats grow and develop enlarged thoraces even as adults (Dawson, 1927).

Lung Fixation and Paraffin Processing

All methods of lung fixation, whether by immersion fixation, intratracheal instillation, vascular perfusion or freezing, produce some artifactual change from the normal in vivo condition of the lung. Vascular perfusion fixation presents technical difficulties in the neonate rat pups because of their small size. Because intratracheal fixation may wash out lung exudates and inflammatory cells, it is generally inappropriate for studies of edema, macrophages, or surfactant (Brain et al., 1984; Renne et al., 2001). Peripheral airspace morphology differs between air-filled and fluid-filled lungs (Gil et al., 1979). Nevertheless, instillation fixation can be well suited to quantitative studies of parenchymal morphology. In their review of rodent lung fixation methods, Renne et al. (2001) concluded that intratracheal fixation provides the best preservation and is the preferred technique for quantitative studies of alveolar morphometry, therefore, this mode of fixation was used for our investigation.

To minimize the formation of microthrombi and occlusion of circulatory beds, rats were heparinized using 1,000 U/kg of heparin (American Pharmaceutical Partners, Schaumberg, IL) injected intraperitoneally (i.p.). The animals were anesthetized and euthanized using 200 mg/kg sodium pentobarbital (Fatal Plus, Vortech Pharmaceuticals, Dearborn, MI) injected i.p. Each rat was then weighed using a Mettler PM 600 balance. The depth of anesthesia was verified by absence of pedal (digital withdrawal) and corneal reflexes before beginning the procedure. The trachea was intubated using heat-flared polyethylene tubing (Becton Dickinson, Sparks, MD) varying in size from PE 50 to PE 205, depending on the age of the rat. The animal was killed by means of severing the aorta and pneumothorax was produced by puncturing the diaphragm from the abdominal side. Fixation of the exposed lungs was performed open chest rather than closed chest. The compliance of the chest wall is age-dependent (Fisher and Mortola, 1980); with the chest wall open, transrespiratory and transpulmonary pressures are essentially equal, thus eliminating this confounding variable. The lungs were fixed using cold 4% paraformaldehyde (Electron Microscopy Science, Hatfield, PA) in phosphate buffered saline (PBS; Invitrogen, Carlsbad, CA), pH 7.4. The fixative was instilled by gravity into the tracheal tubing with a head pressure of 23 cm H_2O. At this pressure, instillation of formalin-based fixative is expected to produce a lung displacement volume approaching total lung capacity (Hayatdavoudi et al., 1980). While fixation at a lower pressure might be of greater physiological relevance, it can result in significant distortion of the lung. On the other hand, fixations at higher pressures (e.g., >25 cm H_2O, or $>$ total lung capacity) can induce leakage, particularly in neonate lungs (Massaro et al., 1985). A leak-free preparation was confirmed by noting whether the transpulmonary pressure remained steady at 23 cm H_2O for 20 min; in these cases, the trachea was then tied off and fixation was continued by immersing the lungs in 4% paraformaldehyde for at least 48 hr at 4°C. In some cases, for rats less than 14 days, the heart was removed before instillation. Over 90% of attempted fixations produced successful, that is, leak-free, lungs; most of the unsuccessful attempts were in neonates.

After fixation, the volume of the fixative-filled lung was determined by volume displacement, assuming that the density of fixative was 1 g/ml. Blocks were cut from the medial portion of the left lung perpendicular to the long axis of the lung for histological processing. The lung was sampled systematically at fixed intervals (>100 μm apart) with the position of the first cut being determined by choosing a random number within the interval (i.e., random start, see Bolender et al., 1993). The tissue was washed, dehydrated through a graded ethanol series, cleared, and paraffin embedded according to standard histological methods. Paraffin blocks were step sectioned, microtomed to ~5μm thickness every 100μm. Sections were affixed to glass microscope slides by baking for at least 4 hr at 50°C.

Immunofluorescent Labeling for α-Smooth Muscle Actin

Sections were deparaffinized using Neo-clear xylene substitute (EMD Chemicals, Gibbstown, NJ), and the tissue was rehydrated through a graded ethanol series and washed in PBS. Because fixation can form cross-links that mask antigenic sites, proteinase K solution (Dako, Carpinteria, CA) was applied for 5 min to break protein cross-links and unmask antigens to enhance immunofluorescent labeling. After additional washing, nonspecific staining was blocked using 5% normal goat serum (Vector Labs, Burlingame, CA) in PBS for 30 min. Mouse monoclonal anti-SMA IgG_{2A} (clone 1A4, Sigma, St. Louis, MO), supplied at a concentration of 2 mg antibody/ml, was diluted 1:100 in blocking buffer and allowed to incubate on sections for 45 min. This antibody is specific for the single isoform of α-SMA. After the primary antibody was washed from the sections, 1 mg/ml stock solution Texas Red–conjugated secondary antibody (Jackson Immunoresearch, West Grove, PA) was diluted 1:500 in blocking buffer and applied for 30 min. A red fluorophore was chosen to avoid potential confounding signal from the innate autofluorescence of lung elastin in the green channel. After thorough washing, slides were cover-slipped using Fluoromount-G mounting media (Electron Microscopy Sciences). The labeling of airway smooth muscle in the sections was used as an internal positive control for the immunolabeling of α-SMA in the lung parenchyma. Negative secondary-only control slides were run omitting the primary antibody from the blocking buffer.

Confocal Laser Scanning Microscopy

Confocal microscopy minimizes out of focus haze, allowing visualization of fine detail that is lost using standard epifluorescence microscopy. Slides were scanned using a Leica TCS NT laser scanning confocal microscope fitted with argon and krypton lasers. Images were recorded using a 40× oil objective lens and tetrarhodamine isothiocyanate filter settings for Texas Red to visualize α-SMA expression. Fluorescein isothiocyanate (FITC) filter settings were used to detect any elastin-based autofluorescence in the lung. No bleed-through across channels was

detected. For the majority of scans, laser power and photomultiplier tube (PMT) settings were held constant. However, although images from neonates and immature rats could be scanned using a constant PMT setting, the much lower α-SMA signal in adults required use of a slightly higher PMT setting in some cases.

Nonoverlapping fields of view of lung parenchyma that lacked readily identifiable airways or major blood vessels were recorded from each slide. The fields containing large vessels and airways were rejected to avoid α-SMA–labeled vascular and airway smooth muscle. Parenchymal fields of view were thus thought to be limited to alveolar septa, alveolar ducts, and capillaries, and, therefore, α-SMA labeling limited to myofibroblasts and pericytes. Any sections containing autofluorescing erythrocytes were rejected. For each individual animal, a minimum of five fields of view was recorded from each of at least six independent (i.e., >100 μm apart in the *z*-axis) lung slabs.

Image Processing and Morphometric Analysis

Areal density and volume proportion (a stereological point counting measure of the number of test points falling on the constituent of interest divided by the number of test points falling on tissue) measures are widely used in the quantification of α-SMA and other lung constituents (see, for example, Escolar et al., 1997; Tanaka et al., 2001; Huang et al., 2007a,2007b). We performed our image processing and quantification using MATLAB software (Mathworks Inc., Natick, MA). Segmentation by means of thresholding of pixel intensity was used to distinguish between area of interest and background. Threshold pixel intensities defining (1) α-SMA–positive tissue, (2) all tissue, and (3) airspace/cellular debris were determined. The segmentation of tissue was automated. The image was further processed by removing clusters of pixels smaller than 2×2 to reduce artifact. The segmented image was smoothed using a five-pixel disc-shaped close operation to clean up small artificial breaks in tissue connectivity. A five-pixel border was also cropped off to remove uncertainty generated by the close operation. The original image was then manually segmented to show α-SMA–positive tissue only. Images used for quantification had no additional processing beyond that described above. In pictures used for display purposes only, the brightness and/or contrast of the entire image were adjusted slightly in some cases to enhance detail.

For each field of view (fov), the two-dimensional (2D) area occupied by all tissue, and the 2D area occupied by α-SMA–positive tissue was measured (area represented the number of pixels multiplied by the pixel size), and the percentage of α-SMA–positive tissue/fov and total tissue/fov calculated. The areal density was found by dividing the number of pixels representing α-SMA by the number representing tissue. Values were averaged to determine the mean α-SMA–positive tissue area/total tissue area for each animal and time point. The total number of fields of view quantified was ~1,000.

Any process of fixation and dehydration likely creates artifact, and paraffin processing, particularly the dehydration steps, can result in tissue shrinkage. Unfortunately, alternative tissue processing methods that avoid paraffin-embedment (see, for example, Dorph-Petersen et al., 2001) were not compatible with other aspects of our study (e.g., cryosectioning did not result in sufficiently preserved morphological detail for our purposes, and resin embedment was not compatible with our immunofluorescent labeling protocol). We took steps to limit dehydration artifact in our paraffin processing, using a slow, gradual ethanol series to minimize shrinkage. Although it is possible that the degree of tissue shrinkage could vary with age, gross measurements of the dimensions of lung slabs before and after processing did not show appreciable age-dependent differences in the degree of shrinkage. No shrinkage correction factor was applied to the morphometric analysis in this study because areal density is a relative rather than absolute measure. We assumed that shrinkage within the tissue was uniform, that is, differences in the extent of shrinkage of SMA-positive and SMA-negative cells were negligible. Any other type of shrinkage, whether associated with age, fixation, or processing, does not contribute artifact to the areal density measure.

Results are reported as means ± 1 SD. To compare values among the different age groups, one-way analysis of variance was used. Means were considered significantly different at a probability level of 5% ($P < 0.05$).

For comparative purposes, for a subset of data, the amount of α-SMA–positive tissue was quantified by an additional technique. A stereological estimate of volume proportion, Vv, was calculated using point counting methods with a test line grid. Vv was determined for the α-SMA–positive tissue and total tissue. The volume fraction of α-SMA (percentage of tissue that was α-SMA–positive) was defined as the number of hits on α-SMA–positive tissue divided by the total number of tissue hits. No significant difference in α-SMA proportion was found between this stereological point-counting estimate using a test grid and the automated full pixel count method described above (results not shown). Thus, all data were analyzed using the automated pixel-counting method.

RESULTS

Concomitant Increases in Lung Volume and Body Mass With Age

To characterize the postnatal growth of the rats in our litters, body weight and fixative-filled lung volume (at an inflation pressure of 23 cm H_2O) were plotted against age. Lung volume was determined by the displacement method, with the density of paraformaldehyde solution at 1 g/ml. Body weight and lung volume both increased with age over the duration of the study (Fig. 1A,B), although not always perfectly proportionately (Fig. 1C). Despite the switch from calorie-dense nursing to rat chow on postnatal day 21, body weight and lung volume both increased rapidly after weaning in our animals. There was a slight though nonsignificant decrease in the ratio of lung volume to body weight with age (Fig. 1C). The lungs were fixed at volumes approaching total lung capacity, and no gross or histological evidence of uneven inflation or fixation was detected.

Antibody Specificity

Both immature and mature rat lungs displayed strong labeling in the smooth muscle of the walls of conducting airways and large blood vessels that were used as an in-

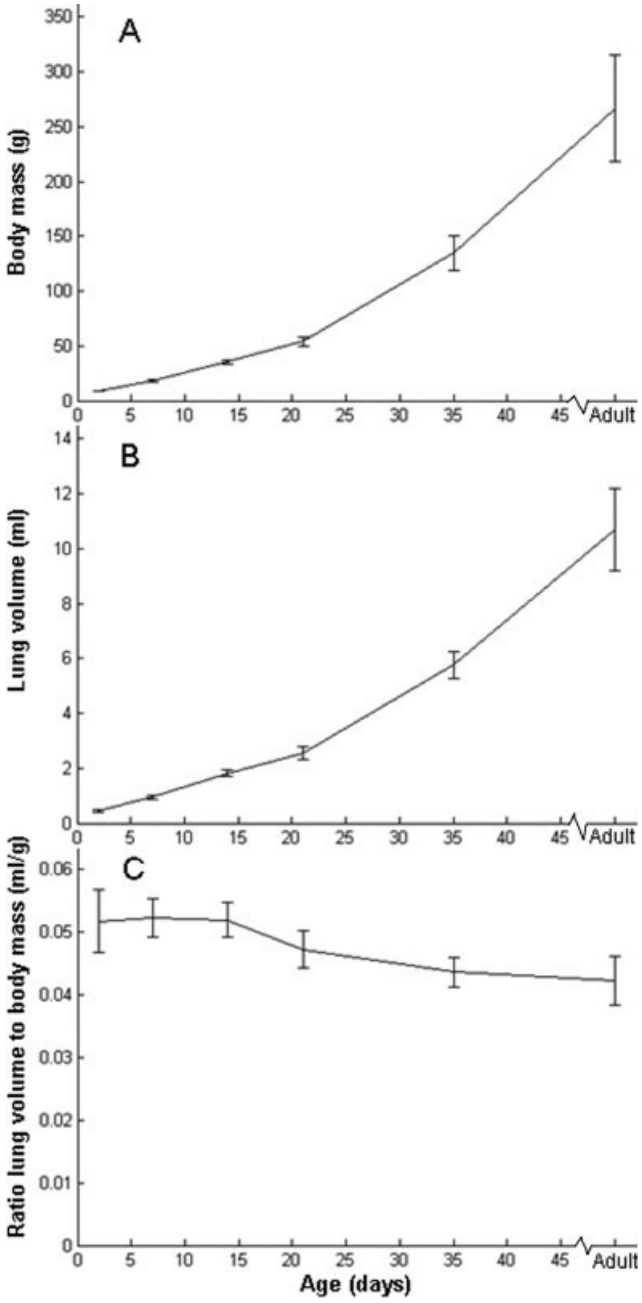

Fig. 1. Change in body mass and fix-filled lung volume with age for outbred Wistar rats. **A:** Body mass vs. age. **B:** Fixative-filled (inflation pressure = 23 cm H_2O) lung volume vs. age. Ratio of lung volume to body mass. **C:** Mean values are plotted for each age group (n = 5 animals/group). Error bars represent ± 1 SD.

ternal positive control for α-SMA reactivity with lung contractile elements. No specific staining was observed in the negative (secondary antibody-only) control slides (Fig. 2D, inset{FIG2}). Elastin-based autofluorescence in the FITC channel often displayed a similar spatial pattern to that of the α-SMA, particularly at the tips of septal crests. Images were checked for bleed-through to ensure that none of this elastin signal was contributing to α-SMA signal in the other channel.

Location and Abundance of α-SMA Expression Changes Through Development

Lung parenchymal tissue immunofluorescently labeled using the antibody to α-SMA was examined in a postnatal series of paraffin-embedded rat lungs. Areas of immunoreactivity within the alveolar parenchyma were observed at all ages examined. Figure 2 shows representative images demonstrating the changing morphology of the lung parenchyma with increasing postnatal age. In the youngest (2-day) rat pups examined, the parenchymal tissue consisted of thick-walled primitive septa with small ridges that protruded slightly into the airspaces. The α-SMA was expressed within the interstitium of the primary septa and at the small ridges (Fig. 2A, asterisk), the presumptive sites of future secondary septum formation. Immature rats had both large elongate, slender α-SMA–positive cells (Figs. 2A, 3, arrowheads; 2-day old) and more round α-SMA–positive cells (Figs. 2A, 3 arrows; 2-day old, 7-day old).

With increasing age and secondary septation, the airspaces became smaller, the alveolar septa more elongate and the alveolar walls thinner. The α-SMA at the leading tips of secondary septa is shown in Figure 2B (arrow, 7-day rat). With septal thinning (Fig. 2C, 21 days), the amount of parenchymal interstitial tissue decreased. The most prominent α-SMA labeling was observed in the young rats. In adult rats, α-SMA staining was fainter and less abundant, and individual concentrations often appeared smaller. The α-SMA was primarily localized to the entrance rings of alveolar ducts (septal ends), and septa bends (Fig. 2D, arrows). Following Oldmixon et al. (2001), a septal bend was defined as border of an alveolar septum that joins one other septum at a definable angle, and a septal end as the free border of an alveolar septum. Rarely, α-SMA was observed at a septal junction, the intersection of three septa. The very large, elongate concentrations of α-SMA, such as found in the immature animals, were not seen in the adults.

Density of α-SMA in the Lung Parenchyma Peaks in 21-Day Old Rats

The fovs used for quantification were selected to avoid large airways and blood vessels, so that only alveolar parenchymal tissue was examined. The total tissue area thus comprised the following cell types: types I and II alveolar epithelial cells, vascular endothelial cells, fibroblasts, myofibroblasts, pericytes, and macrophages.

The images of α-SMA–labeled parenchyma were digitally analyzed to determine changes in the quantity of α-SMA over time. Figure 3 illustrates the image processing steps used to ascertain α-SMA areal density. The left hand column shows representative confocal images of immature rat lung parenchyma before any processing. Each image was segmented to obtain areal values of tissue-only and α-SMA–positive tissue only. The resultant segmentation for each original image is illustrated in the middle and right-hand columns.

The amount of SMA in the lung parenchyma, as estimated by the areal density of α-SMA–positive staining in alveolar interstitium, is relatively modest, always <8% of the total tissue area. In neonate (2-day) rats, an average of ~4% of the parenchymal tissue was positive for α-SMA. The amount of α-SMA increased dramati-

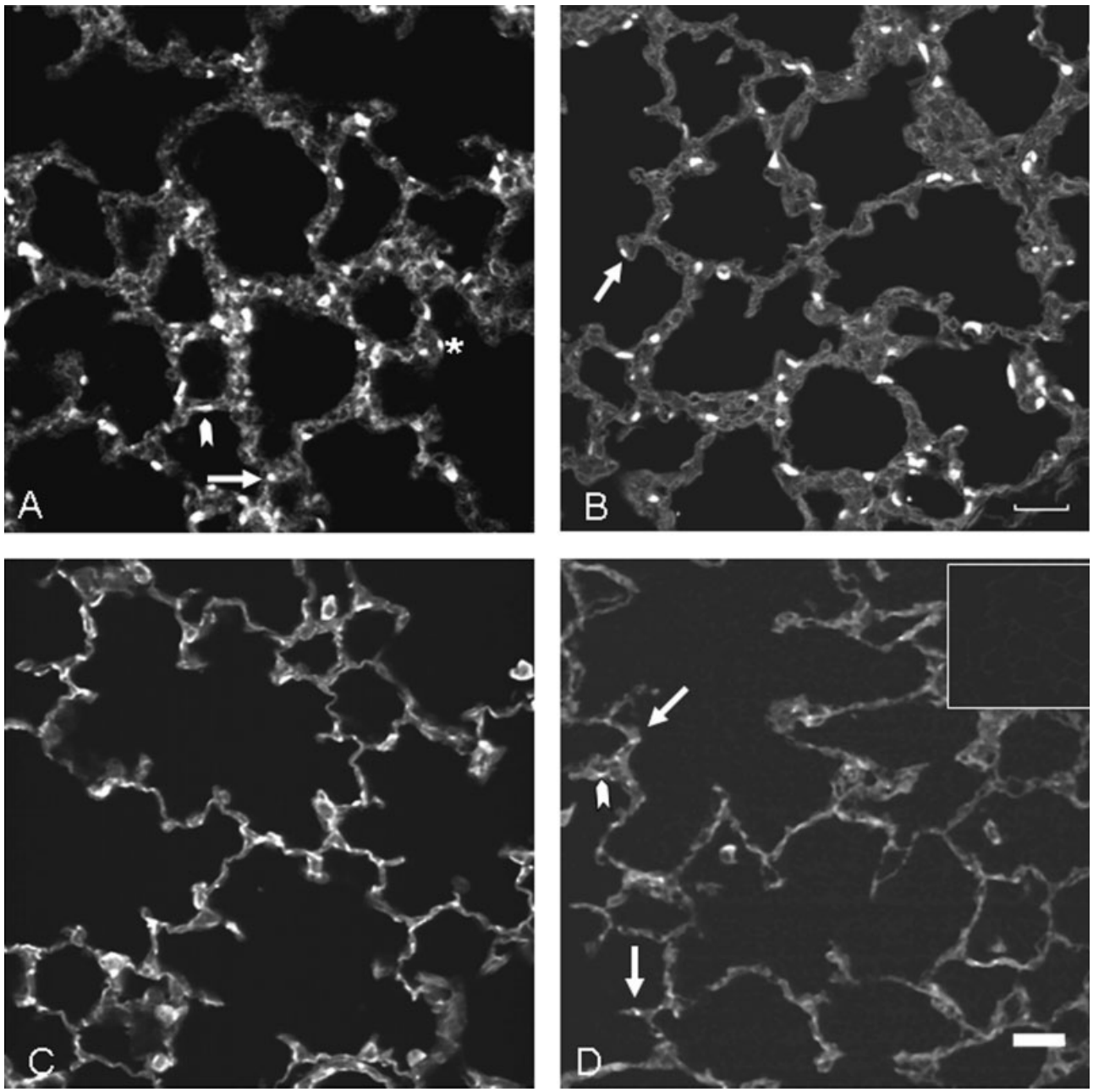

Fig. 2. Representative images of rat lung parenchyma showing changes in morphology with age. Paraffin sections immunofluorescently labeled with alpha–smooth muscle actin (α-SMA) and Texas Red. **A:** Two-day-old rat (period of lung expansion) with large concentrations of α-SMA within the thick primitive septa. Elongate concentration of α-SMA (arrowhead); round concentration of α-SMA (arrow). The asterisk indicates α-SMA at the septal ridge. **B:** Seven-day rat (period of septation) with α-SMA at the septal tip (arrow). **C:** Twenty-one-day rat with a thinned alveolar septa. **D:** An adult rat with α-SMA at alveolar ends and bends (arrows) and presumed pericyte location (arrowhead). Scale bar = 25 μM. Negative control shown in inset of D.

cally during the first 3 weeks, particularly from the second to third week (Fig. 4). The peak at 21 days was followed by a continual decline toward adulthood. The percentage of α-SMA–positive parenchyma ranged from a low of ~3% in adults to a high of a little over 7% on postnatal day 21. The amount of α-SMA at 21 days is significantly higher than that of the younger rats sampled or adults ($P < 0.05$).

DISCUSSION

In the present study, we quantified the contractile element content of the lung parenchyma through digital analysis of confocal images of tissue immunofluorescently labeled for α-SMA. To our knowledge, this is the first study to systematically quantify α-SMA content in the alveolar septa through postnatal ontogeny. The main

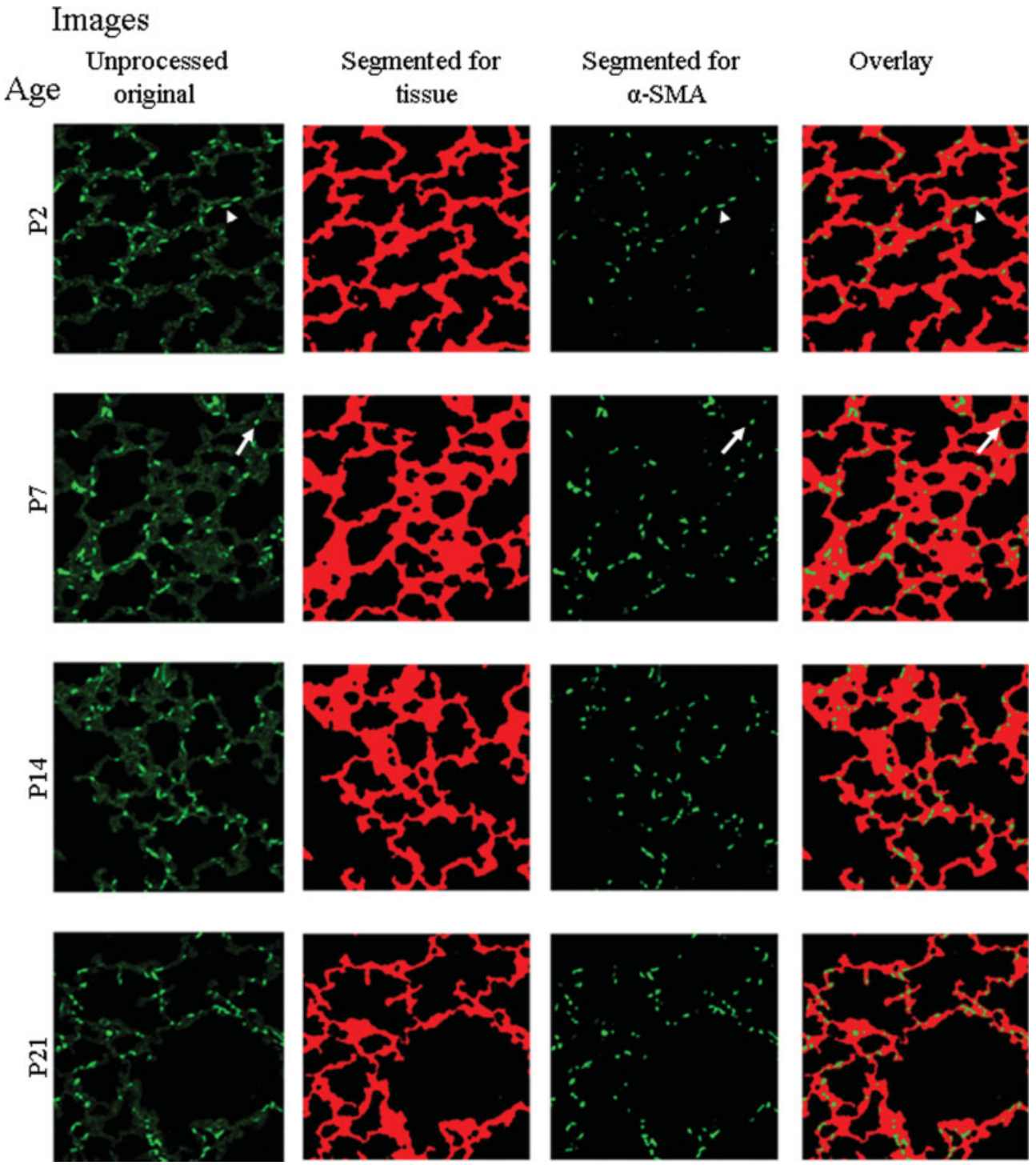

Fig. 3. Image processing of rat lung parenchyma immunofluorescently labeled with alpha–smooth muscle actin (α-SMA) and Texas Red. The left-hand column shows original, unprocessed representative confocal images from 2-day, 7-day, 14-day, and 21-day rats. Middle columns show the same images automatically segmented to remove background and show total tissue (red), and manually segmented to show α-SMA–positive tissue only (green). Right-most column shows overlay of α-SMA (green) and tissue (red). Arrowheads indicate an elongated, slender concentration of α-SMA; arrows indicate a more rounded α-SMA–positive concentration.

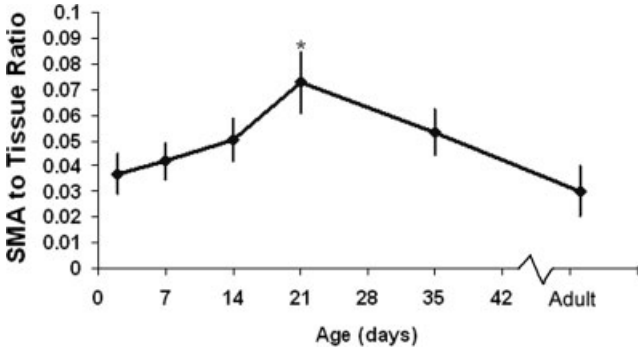

Fig. 4. Mean ratio of alpha–smooth muscle actin (α-SMA) -positive tissue area/total parenchymal tissue area vs. age. Values were calculated using segmented images from a postnatal series of rat lungs. Mean values are plotted for each age group, n = 5 animals per group. Error bars represent ± 1 SD. The proportion of parenchymal tissue that was α-SMA–positive in 21-day old rats was significantly higher than that of younger or adult rats ($P < 0.05$).

finding of our investigation was that the relative amount of α-SMA–positive tissue increases rapidly from the neonatal stage, particularly from 14 to 21 days, peaks in 3-week-old rats, then declines toward adulthood. The timing of this peak is consistent with the extensive developmental remodeling occurring around this period. The phase of active, myofibroblast-dependent alveolarization in the first 2 weeks, followed by loss of tissue area by means of septal thinning occurring through the third week (Burri, 2006), likely contributes to this peak in the ratio of α-SMA to tissue area at 21 days.

Alpha-SMA Distribution Changes During Lung Maturation

Whereas α-SMA expression begins relatively early in lung development in the smooth muscle of airways and large blood vessels, α-SMA in alveolar myofibroblasts and pericytes has not been detected until after birth in rats (Jostarndt-Fogen et al., 1998). Jostarndt-Fogen et al. detected only faint staining at 8-hr postpartum, but by the next time point sampled, 3 days, staining had become intense. We found that intense staining was already present by the second postnatal day (Figs. 2A, 3). Rats younger than 2 days were not investigated in our study due to the technical difficulty of obtaining leak-free lung fixation at this small size.

The spatial and temporal distribution of α-SMA in the maturing lung that was found in this study confirmed and extended the findings of previous investigators. Consistent with data from cryosectioned material (Yamada et al., 2005), in our paraffin sections, we found that the thick-walled primary septa of neonate rats contained slender α-SMA–positive interstitial cells (Figs. 2A, 3, 2-day rat). Postnatally, there was also a population of round cells with α-SMA at tips of septa (Fig. 2B; 7 day rat), as well as elongate cells with α-SMA in the interstitium. Here, we term these two populations of α-SMA–positive cells myofibroblast-like cells. In the adult rat lung, Yamada et al. (2005) found that α-SMA–positive cells were restricted to alveolar ends. We, however, also found α-SMA–positive cells in the alveolar bends of adult rats. This finding is consistent with the observations of Oldmixon et al. (2001), and with their argument that septal bends and ends are analogous structures insofar as they necessarily contain stress-bearing tissue, unlike the junctions where three septa meet. The population of elongate α-SMA–positive cells found within the immature alveolar interstitium was not present in the mature rats of Oldmixon et al., as α-SMA in the alveolar septa was restricted to alveolar ends and bends, as in our study. This finding suggests that this population of elongate interstitial α-SMA–positive cells may be lost with maturity, as suggested by Yamada et al. (2005). The similar spatial patterns we observed for both α-SMA expression and elastin autofluorescence, for example, at the tips of alveolar crests, are consistent with the myofibroblasts' role in tropoelastin synthesis.

α-SMA Areal Density Changes During Lung Maturation

The observed rapid increase in the proportion of parenchymal tissue that was α-SMA–positive until the 21st day, followed by diminishment toward maturity, parallels the period of rapid septation followed by the slowing of alveolarization and septal thinning toward adulthood. Previous studies did not quantify the amount of α-SMA specifically within the alveolar interstitium in developing rats. Oldmixon et al. (2001) investigated the distribution of contractile elements, as estimated by the areal density of α-SMA, for the airways, alveolar ducts, and blood vessels of adult rats only. Tanaka et al. (2001) examined a postnatal series of rat lung parenchymal strips starting at 10 days, but airways and large blood vessels were not excluded from this analysis. They found that the volume proportion of α-SMA–positive tissue was 10.7% in 10- to 14-day-old rats, 7.3% in 21-day rats, and 7.8% in 8-week rats. The extent of this change occurring within the alveolar interstitium, rather than in the smooth muscle of the airways and vessels, is unknown, and likely accounts for the differences in these results from our own. Unlike Tanaka et al., we found that the proportion of α-SMA increased from the second to third week (Fig. 4). Additionally, the α-SMA percentage for the adult by Tanaka et al. is a great deal higher than that found in our study, suggesting that the investment of airways and large vessels with smooth muscle contributes more α-SMA to the deep lung per unit area than the alveolar septa and ducts. Because our study was concerned with the major events of lung restructuring occurring during early postnatal development, we did not sample into old age, but changes in the α-SMA content continue even late in life. The trend of decreasing α-SMA with maturation may reverse with advanced age: the number of α-SMA–positive septal tips increased in rats >20 months (Yamamoto et al., 2003).

Types of α-SMA–Positive Cells

The α-SMA antibody is known to mark airway and vascular smooth muscle cells, myofibroblasts associated with development, injury, and BPD (Toti et al., 1997), and depending on tissue type and species, microvascular pericytes. The nomenclature in the literature is not uniform. Nonpericyte α-SMA–positive cells in the lung parenchyma have variously been called precursor myofi-

broblasts, myofibroblasts, contractile interstitial cells and smooth muscle cells (see for example, Mitchell et al., 1989; Kapanci et al., 1992). Pericytes themselves are classified by some investigators as a subtype of myofibroblast (Kapanci et al., 1992). The interrelated ontogeny of pericytes, myofibroblasts, and smooth muscle cells is complex and largely unknown. The differences between these cell types are continuous rather than discrete, so discriminating among these cells types can be challenging; for example, no pericyte-specific markers are available.

The α-SMA–positive myofibroblast-like cells labeled in this study thus likely represent more than a single population of contractile cells, depending on their spatial and temporal distribution. Because large airways and blood vessels were excluded from our analysis, the populations of α-SMA–expressing cells we found are most likely to be restricted to development-associated myofibroblasts and microvascular pericytes in the interstitium of the alveolar wall and, in adults, smooth muscle cells forming the rings surrounding the alveolar entrances. The identification and subdivision of the observed myofibroblast-like cells to microvascular pericytes vs. development-associated myofibroblasts was beyond the scope of the current study, but it should be noted that in addition to labeling smooth muscle cells and myofibroblasts, α-SMA is known to label pericytes in rat lung parenchyma (Kapanci et al., 1992; Fehrenbach et al., 1999; Zhang et al., 1999). Pericytes are not expected to contribute to the majority of α-SMA in the lung parenchyma; Weibel (1974) found that pericyte-coverage in adult lungs was very low compared to that of systemic vessels. Nonetheless, a subset of the spindle-shaped α-SMA–positive cells we observed within the airspace walls, not in the region of prospective alveolar ducts, were likely pericytes. The occasional α-SMA signal we observed at alveolar junctions is likely due to pericytes (Kapanci et al., 1992). Because pericytes are markers of blood vessel maturity, and vascular development is known to be intimately connected to alveolarization and BPD (Stenmark and Balasubramaniam, 2005), pericyte prevalence is also expected to vary with age, presumably increasing as the vascular bed matures. Although the data are not available for rat, such a trend has been found in bovine lung (Sims and Westfall, 1983). Thus, while some populations of myofibroblast-like cells may diminish during postnatal development, another population may increase in number with maturation. The proportion of α-SMA decreased in our study after 21 days, following the period during which the majority of microvessel maturation takes place.

Speculated Functional Importance of Contractile Elements in the Lung Parenchyma

Open questions remain concerning the functions of the α-SMA–positive lung parenchymal cells. During development, myofibroblasts are required for normal septation, and the addition of pericytes around microvessels is associated with blood vessel maturity. Disregulation of the normal quantity and functioning of α-SMA–positive cells is associated with the pathogenesis of several diseases, both in adult and immature animals. In the healthy adult, α-SMA–positive contractile cells are no longer needed for lung morphogenesis, but appear to still play a role in lung function. Pericyte contractility is thought to be involved in regulating changes in microvessel permeability, such as those accompanying lung inflammation (Donoghue et al., 2006). Sims and Westfall (1983) hypothesized that pericytes may profoundly influence lung parenchymal shape and function by altering microvascular blood flow. Although there is not yet definitive in vivo data, modeling indicates that the quantity of contractile tissue within the alveolar entrance rings contributes to pressure–volume and geometric hysteresis during breathing (Kojic et al., 2006). We confirmed SMA expression at septal end and bends, sites of elastin and collagen-rich cables of proposed mechanical significance (Oldmixon et al., 2001). Lindahl and Betsholtz (1998) generalized that both α-SMA–expressing cell types, pericytes and myofibroblasts, are important in maintaining the mechanical stability of small-diameter hollow structures, microvessels and alveoli, respectively. The functional effect of the changes in α-SMA content that accompany lung maturation is an area requiring investigation.

Comparison to Human Lung Parenchyma

The rat lung is arguably the most widely investigated laboratory model for human pulmonary development (Burri, 1997), and the extent of change in many lung parameters (e.g., relative increase in lung volume, septal volume, and alveolar surface area) from birth to adulthood are remarkably similar in rats and humans (Zeltner et al., 1987), though the timing of events varies across species. Our time points were chosen to sample major periods of structural change in the lung. The timing of the major lung developmental stages in mice, another widely used model organism in pulmonary studies, is very similar (Dietert et al., 2000). The 2-day rat lung represents a prenatal saccular stage of human lung development. We found parenchymal α-SMA expression at this age; α-SMA immunoreactivity has also been demonstrated in the septa of human lungs at 28 weeks of gestation (Toti et al., 1997). At 7 days, the rat lung is in the midst of a period of rapid alveolar septation. The postnatal human lung shows a similar pattern of α-SMA expression at septal crests (Leslie et al., 1990). At 14 days, bulk alveolarization in the rat lung is diminished and lung development proceeds predominantly by microvascular maturation and septal thinning (Burri, 2006), producing a miniature version of adult lung morphology after 3 weeks in rats and ~3 years in humans (Burri, 2006). Alveoli are numerous at this stage, but they have not yet grown to their adult size. This was the period of peak α-SMA density in rat lungs; we are not aware of quantitative data for the α-SMA content of human lungs at this age. At 35 days, rat alveoli are still increasing in size; Dietert et al. (2000) estimate that alveolar expansion occurs from ages 2 to 8 years in humans. In adults (>100 days in our study), the alveolar parenchyma has reached its mature dimensions (Burri, 1997, 2006); lung growth is complete in humans by 18–20 years (Levitzky, 1984). The α-SMA is less abundant in adults compared with younger rats; similarly, the number of α-SMA–positive cells per unit area of in 22-year-old humans is reduced compared with the childhood condition, and the parenchymal distribution restricted to alveolar ducts and pericytes (Leslie et al., 1990).

To conclude, we found that the proportion of α-SMA–positive alveolar parenchyma increased from neonates to 3 weeks of age, then decreased toward adulthood. The alveolar development occurring between birth and 21-days differs dramatically from that occurring after the 3-week mark. The rising level of α-SMA is presumably related to the period of active septation and elastin deposition in the first 2 weeks of life. Alveolar wall thinning in the third week decreases the amount of parenchymal tissue, contributing to the peak in α-SMA area to total tissue area at 21 days. A population of the α-SMA–expressing cells in the alveolar interstitium that is found in immature animals appears to be lost with maturation, resulting in a decreased amount of α-SMA in adults. Greater understanding of the changes in distribution and quantity of α-SMA that accompany alveolar maturation provides the groundwork for future investigations of the functional consequences of such change during postnatal ontogeny, as well as providing base line values for comparison against pathology and experimental manipulation.

ACKNOWLEDGMENTS

We thank the Dana Farber/Harvard Cancer Center Rodent Histopathology Core as well as Ms. Katie Szymanska, for technical assistance.

LITERATURE CITED

Bolender RP, Hyde DM, Dehoff RT. 1993. Lung morphometry: a new generation of tools and experiments for organ, tissue, cell, and molecular biology. Am J Physiol 265(Pt 1):L521–L548.

Bostrom H, Willetts K, Pekny M, Leveen P, Lindahl P, Hedstrand H, Pekna M, Hellstrom M, Gebre-Medhin S, Schalling M, Nilsson M, Kurland S, Tornell J, Heath JK, Betsholtz C. 1996. PDGF-A signaling is a critical event in lung alveolar myofibroblast development and alveogenesis. Cell 85:863–873.

Bourbon J, Boucherat O, Chailley-Heu B, Delacourt C. 2005. Control mechanisms of lung alveolar development and their disorders in bronchopulmonary dysplasia. Pediatr Res 57:38R–46R.

Brain JD, Gehr P, Kavet I. 1984. Airway macrophages. The importance of the fixation method. Am Rev Respir Dis 129:823–826.

Burri PH. 2006. Structural aspects of postnatal lung development - alveolar formation and growth. Biol Neonate 89:313–322.

Burri PH. 1997. Structural aspects of prenatal and postnatal development and growth of the lung. In: McDonald JA, editor. Lung growth and development. New York: Dekker. p 1–35.

Burri PH, Dbaly J, Weibel ER. 1974. The postnatal growth of the rat lung. I. Morphometry. Anat Rec 178:711–730.

Dawson AB. 1927. Further studies on the epiphyses of the albino rate skeleton, with special reference to the vertebral column, ribs, sternum and girdles. Anat Rec 34:351–363.

Demayo F, Minoo P, Plopper CG, Schuger L, Shannon J, Torday JS. 2002. Mesenchymal-epithelial interactions in lung development and repair: are modeling and remodeling the same process? Am J Physiol Lung Cell Mol Physiol 283:L510–L517.

Dietert RR, Etzel RA, Chen D, Halonen M, Holladay SD, Jarabek AM, Landreth K, Peden DB, Pinkerton K, Smialowicz RJ, Zoetis T. 2000. Workshop to identify critical windows of exposure for children's health: immune and respiratory systems work group summary. Environ Health Perspect 108(Suppl 3):483–490.

Dorph-Petersen KA, Nyengaard JR, Gundersen HJ. 2001. Tissue shrinkage and unbiased stereological estimation of particle number and size. J Microsc 204:232–246.

Donoghue L, Tyburski JG, Steffes CP, Wilson RF. 2006. Vascular endothelial growth factor modulates contractile response in microvascular lung pericytes. Am J Surg 191:349–352.

Escolar JD, Tejero C, Escolar MA, Montalvo F, Garisa R. 1997. Architecture, elastic fiber, and collagen in the distal air portion of the lung of the 18-month-old rat. Anat Rec 248:63–69.

Fehrenbach H, Kasper M, Haase M, Schuh D, Muller M. 1999. Differential immunolocalization of VEGF in rat and human adult lung, and in experimental rat lung fibrosis: light, fluorescence, and electron microscopy. Anat Rec 254:61–73.

Fisher JT, Mortola JP. 1980. Statics of the respiratory system in newborn mammals. Respir Physiol 41:155–172.

Gil J, Bachofen H, Gehr P, Weibel ER. 1979. Alveolar volume-surface area relation in air- and saline-filled lungs fixed by vascular perfusion. J Appl Physiol 47:990–1001.

Hayatdavoudi G, Crapo JD, Miller FJ, O'Neil JJ. 1980. Factors determining degree of inflation in intratracheally fixed rat lungs. J Appl Physiol 48:389–393.

Huang K, Mitzner W, Rabold R, Schofield B, Lee H, Biswal S, Tankersley CG. 2007a. Variation in senescent-dependent lung changes in inbred mouse strains. J Appl Physiol 102:1632–1639.

Huang K, Rabold R, Schofield B, Mitzner W, Tankersley CG. 2007b. Age-dependent changes of airway and lung parenchyma in C57BL/6J mice. J Appl Physiol 102:200–206.

Jostarndt-Fogen K, Djonov V, Draeger A. 1998. Expression of smooth muscle markers in the developing murine lung: potential contractile properties and lineal descent. Histochem Cell Biol 110:273–284.

Kapanci Y, Ribaux C, Chaponnier C, Gabbiani G. 1992. Cytoskeletal features of alveolar myofibroblasts and pericytes in normal human and rat lung. J Histochem Cytochem 40:1955–1963.

Kim N, Vu TH. 2000. Parabronchial smooth muscle cells and alveolar myofibroblasts in lung development. Birth Defects Res C Embryo Today 78:80–89.

Kohn DF, Clifford CB. 2002. Biology and diseases of rats. In: Fox JG, Anderson LC, Loew FM, Quimby FW, editors. Laboratory animal medicine. 2nd ed. New York: Academic Press. p. 121–165.

Kojic M, Butler J, Vlastelica I, Stojanovic B, Rankovic V, Tsuda A. 2006. Geometric hysteresis of alveolated duct architecture. FASEB 20:A1258–A1259.

Le Cras TD, Kim DH, Gebb S, Markham NE, Shannon JM, Tuder RM, Abman SH. 1999. Abnormal lung growth and the development of pulmonary hypertension in the Fawn-Hooded rat. Am J Physiol 277(Pt 1):L709–L718.

Leslie KO, Mitchell JJ, Woodcock-Mitchell JL, Low RB. 1990. Alpha smooth muscle actin expression in developing and adult human lung. Differentiation 44:143–149.

Levitzky MG. 1984. Effects of aging on the respiratory system. Physiologist 27:102–107.

Lindahl P, Betsholtz C. 1998. Not all myofibroblasts are alike: revisiting the role of PDGF-A and PDGF-B using PDGF-targeted mice. Curr Opin Nephrol Hypertehs 7:21–26.

Lindahl P, Karlsson L, Hellstrom M, Gebre-Medhin S, Willetts K, Heath JK, Betsholtz C. 1997. Alveogenesis failure in PDGF-A-deficient mice is coupled to lack of distal spreading of alveolar smooth muscle cell progenitors during lung development. Development 124:3943–3953.

Massaro D, Teich N, Maxwell S, Massaro GD, Whitney P. 1985. Postnatal development of alveoli. Regulation and evidence for a critical period in rats. J Clin Invest 76:1297–1305.

McHugh KM. 1995. Molecular analysis of smooth muscle development in the mouse. Dev Dyn 204:278–290.

Mitchell J, Woodcock-Mitchell J, Reynolds S, Low R, Leslie K, Adler K, Gabbiani G, Skalli O. 1989. Alpha-smooth muscle actin in parenchymal cells of bleomycin-injured rat lung.Lab Invest 60:643–650.

Mitchell JJ, Reynolds SE, Leslie KO, Low RB, Woodcock-Mitchell J. 1990. Smooth muscle cell markers in developing rat lung. Am J Respir Cell Mol Biol 3:515–523.

Oldmixon EH, Carlsson K, Kuhn C, Butler JP, Hoppin FG. 2001. alpha-Actin: disposition, quantities, and estimated effects on lung recoil and compliance. J Appl Physiol 91:459–473.

Renne R, Fouillet X, Maurer J, Assaad A, Morgan K, Ha F, Nikula K, Gillet N, Copley M. 2001. Recommendation of optimal method for formalin fixation of rodent lungs in routine toxicology studies. Toxicol Pathol 29:587–589.

Rishikof DC, Lucey EC, Kuang PP, Snider GL, Goldstein RH. 2006. Induction of the myofibroblast phenotype following elastolytic injury to mouse lung. Histochem Cell Biol 125:527–534.

Schittny JC, Djonov V, Fine A, Burri PH. 1998. Programmed cell death contributes to postnatal lung development. Am J Respir Cell Mol Biol 18:786–793.

Sims DE, Westfall JA. 1983. Analysis of relationships between pericytes and gas exchange capillaries in neonatal and mature bovine lungs. Microvasc Res 25:333–342.

Skalli O, Ropraz P, Trzeciak A, Benzonana G, Gillessen D, Gabbiani G. 1986. A monoclonal antibody against alpha-smooth muscle actin: a new probe for smooth muscle differentiation. J Cell Biol 103:2787–2796.

Soutiere SE, Mitzner W. 2006. Comparison of postnatal lung growth and development between C3H/HeJ and C57BL/6J mice. J Appl Physiol 100:1577–1583.

Stenmark KR, Balasubramaniam V. 2005. Angiogenic therapy for bronchopulmonary dysplasia: rationale and promise. Circulation 112:2383–2285.

Tanaka R, Al-Jamal R, Ludwig MS. 2001. Maturational changes in extracellular matrix and lung tissue mechanics. J Appl Physiol 91:2314–2321.

Tomasek JJ, Gabbiani G, Hinz B, Chaponnier C, Brown RA. 2002. Myofibroblasts and mechanoregulation of connective tissue remodeling. Nat Rev Mol Cell Biol 3:349–363.

Torday J, Rehan VK. 2007. The evolutionary continuum from lung development to homeostasis and repair. Am J Physiol Lung Cell Mol Physiol 292:L608–L611.

Toti P, Buonocore G, Tanganelli P, Catella AM, Palmeri ML, Vatti R, Seemayer TA. 1997. Bronchopulmonary dysplasia of the premature baby: an immunohistochemical study. Pediatr Pulmonol 24:22–28.

Warburton D, Tefft D, Mailleux A, Bellusci S, Thiery JP, Zhao J, Buckley S, Shi W, Driscoll B. 2001. Do lung remodeling, repair, and regeneration recapitulate respiratory ontogeny? Am J Respir Crit Care Med 164:S59–S62.

Weibel ER. 1974. On pericytes, particularly their existence on lung capillaries. Microvasc Res 8:218–235.

Yamada M, Kurihara H, Kinoshita K, Sakai T. 2005. Temporal expression of alpha-smooth muscle actin and drebrin in septal interstitial cells during alveolar maturation. J Histochem Cytochem 53:735–744.

Yamamoto Y, Tanaka A, Kanamaru A, Tanaka S, Tsubone H, Atoji Y, Suzuki Y. 2003. Morphology of aging lung in F344/N rat: alveolar size, connective tissue, and smooth muscle cell markers. Anat Rec A Discov Mol Cell Evol Biol 272:538–547.

Zeltner TB, Caduff JH, Gehr P, Pfenninger J, Burri PH. 1987. The postnatal development and growth of the human lung. I. Morphometry. Respir Physiol 67:247–267.

Zhang Y, Xiong M, Che D, Yuan Y. 1999. Establishment of the culture technique of pulmonary vascular pericytes and its identification in rats. J Tongji Med Univ 19:23–26.